Dual-Helicity Decoupled Coding Metasurface for Independent Spin-to-Orbital Angular Momentum Conversion

Guowen Ding, Ke Chen,* Xinyao Luo, Junming Zhao, Tian Jiang, and Yijun Feng†
School of Electronic Science and Engineering, Nanjing University, Nanjing 210093, China

(Received 16 January 2019; revised manuscript received 5 March 2019; published 15 April 2019)

Controlling spin-to-orbital angular momentum (OAM) conversion plays an important role in many optical and wireless communication applications. While independent control of different circular-polarized (CP) wavefronts could offer an ultimate degree of freedom in designing advanced multifunctional spin devices, most metasurfaces only provide dependent wavefront control. We propose a reflective dual-helicity decoupled coding metasurface to completely realize independent control of OAM vortices for two orthogonal helicities. The element combines both the propagation phase and geometric phase, thus overcoming the inherent limitation encountered by conventional geometric phase elements whose phase responses are constrained to be opposite values for different CP wavefronts. Several design examples for independently generating OAM vortices in the microwave region are presented where a free combination of different OAM modes, helicity, as well as complex spatial beam editing can be fully achieved. Experiments show good agreements with the full-wave simulations, successfully verifying the design theory. The proposed method could offer an alternative platform for designing high-performance devices with independent CP wavefront manipulations, which may enhance the information capacity of metasurfaces and trigger versatile electromagnetic (em) wave function integrations for advanced compact systems.

DOI: 10.1103/PhysRevApplied.11.044043

I. INTRODUCTION

Since Maxwell's equations were developed and radio waves were first produced in the 19th century, unremitting efforts have been made to pursue arbitrary control of electromagnetic (em) waves. In recent years, metamaterials with artificially engineered structures show great potential in manipulating em waves due to their peculiar characteristics that are not available with natural materials such as negative permittivity, negative permeability, and so on [1–4]. Although the emergence of metamaterials has significantly enhanced the ability to manipulate em waves, the bulky three-dimensional (3D) configuration, complicated design, and considerable insertion loss still hinder their further practical applications. Metasurfaces, as the planar version of metamaterials, could potentially overcome these severe limitations due to their advantages of intrinsic simple geometric configuration and ultimate low profile [5–11]. In addition, by introducing field discontinuities across the interface, the amplitude, phase, and polarization of em waves can be controlled at will by metasurfaces within subwavelength thicknesses. Up until now, numerous fascinating phenomena or applications have been demonstrated including anomalous reflection and/or refraction [4,12–14], wave plates [15,16], focusing lenses [17,18], holographic imagers [19,20], and so on.

To meet the explosive demands for large channel capacity in optical and wireless communications, many efforts have been realized such as multi-input multi-output (MIMO) techniques [21,22], multibeam and multifunctional devices [23,24], and even reconfigurable metadevices loaded with active components [17,25], and so on. Recently, vortex waves carrying orbital angular momentum (OAM) show promising prospects in tremendously enhancing the data capacity of communication systems [26–31] because their multiple orthogonal modes can simultaneously transfer at the same frequency in a single communication channel, offering alternative and flexible degrees of freedom. The spiral wavefronts of vortex beams have azimuthal phase evolution around the propagation direction with the form $e^{-il\varphi'}$ carrying the OAM of $l\hbar$, where l represents the topological charge of the OAM mode, φ' is the azimuthal angle around the propagation direction, and $\hbar$ is the reduced Planck's constant [30–32]. Single or diverse mixed-mode OAM beams have been achieved by metasurface designs both in transmissive and reflective modes [31–34]. In particular, OAM generation has also been extended to anisotropic forms for further enhancing the information capacity of the metasurfaces without increasing the space of the device, thus meeting the increasingly huge data link budget required by modern science and technology. For instance, a dual-polarized metasurface can reflect em waves with different OAM modes depending on the incident polarization [34,35]. However, these metasurfaces only provide possibilities in

*ke.chen@nju.edu.cn
†yifeng@nju.edu.cn

controlling the linear polarization, with severe limitations for practical applications [34,35], because spin angular momentum (SAM), expressed as $\sigma\hbar$ [$\sigma = \pm 1$, corresponds to the helicity of a circular-polarized (CP) wavefront], is also an important component for angular momentum. In this regard, geometric phase (or Pancharatnam-Berry phase) metasurfaces have been recently introduced for achieving spin-to-OAM conversion for two orthogonal helicities [36–40]. With spatially interleaved phase profiles or multiplexing techniques, the geometric phase metasurface can generate the desired multichannel multi-OAM beams for certain helical waves [41–43]. Nevertheless, the topological charge of OAM beams will be exactly inversed once the incident helicity is changed, indicating that only spin-locked or dual-helicity coupled OAM beams can be achieved. The underlying reason for this effect is due to the inherent feature of geometric phase metasurfaces that only provide exactly inversed spatial phase profiles for orthogonal spins. Such limitations would further hinder their uses in many real-world applications. Therefore, completely independent control of the wavefront and OAM modes for two different helicities is still a problem, and efforts should be made to seek deployable solutions.

In this paper, we propose a reflective coding metasurface to independently tune the phase functions for CP wavefronts with two orthogonal helicities, and then demonstrate a completely dual-helicity decoupled OAM-beam generation. A general theoretical framework is developed to analyze the design principle of a metasurface element with such helicity-irrelevant phase functions working in the reflective mode. We then design a metasurface element with low cross talk for two orthogonal linear-polarized waves, which will further simplify the design process for independent spin-to-OAM conversion. In particular, complex wavefront multiplexing, superimposing of multi-OAM modes, and spatial-beam editing can be independently realized in each helicity channel through judicious design of the spatial phase profiles on the metasurface. The proposed metasurface will greatly increase the channel capacity of communication systems. Experiments are carried out in the microwave region with the center frequency set as 16 GHz, and good agreements are observed between simulated and measured results. The proposed coding metasurface opens an alternative way for independently manipulating the CP wavefronts, in addition to previous bare propagation phase or geometric phase encoded metasurfaces.

II. THEORETICAL ANALYSIS AND ELEMENT DESIGN

Since the scattering pattern of a reflective metasurface is closely dependent on the output wavefront emerging from the spatially varying metasurface elements [8,13], the combination of two distinct phase responses operating with orthogonal-polarized circular waves on a same metasurface element is the key step for realization of the proposed metasurface. Unfortunately, conventional geometric phase elements have inherent limitations in that they are constrained to be conjugate values for two orthogonal circular incidences [44], further leading to the OAM modes produced by the whole metasurface being conjugate values for two helicity waves [9]. To solve this problem, we have designed a kind of meta-atom whose reflection phase responses for arbitrary helicity can be independently controlled at will by introducing both the propagation phase and geometric phase. Actually, for an arbitrary meta-atom, the phase responses can be divided into two components, namely, the propagation phase and geometric phase [26,45]. For the propagation phase alone, the phase response for linear polarization can be changed by adjusting the structural parameters of the meta-atom with a fixed angular orientation. Therefore, through careful design, arbitrary and independent propagation phase responses for both x and y polarized waves may be obtained by anisotropic meta-atoms. On the other hand, for the geometric phase alone, an additional phase shift of $\varphi = \pm 2\alpha$ can be imparted onto the output wave as the geometric phase meta-atom is self-rotated by an angle of α, where the sign "+" or "−" corresponds to the results under left-handed circular-polarized (LCP) or right-handed circular-polarized (RCP) wave incidence, respectively. By combining these two phase components, metasurfaces operated in transmission mode have been successfully demonstrated for independent control of the circular transmitted wavefronts [26,45]. In order to simplify the design process, we use the concept of coding metasurfaces by designing digital metaparticles with discrete phase functions [46–50]. Coding the metasurfaces could bring about the thrilling perspective of building connections between a physical metasurface and digital coding sequence, as well as information science.

Figure 1 shows the schematic of the proposed coding metasurface for independently generating OAM functions converted from the incident CP wavefront. The coding metasurface shown in Fig. 1 consists of 40×40 coding metasurface elements, with a phase interval of 45° for 3-bit coding elements. Under the illumination of a LCP wave, a reflective vortex beam with the OAM mode $l = 2$ is generated and redirected toward the surface normal direction, while the one with the OAM mode $l = 0$ is along the direction of 51° deviated from the surface normal in the xoz plane. The red arrows in Fig. 1(a) indicate the beam scattering directions. When the incidence is switched to the RCP state, two vortex beams with OAM mode $l = \pm 1$ are generated and scattered toward the directions of -11° and 23° [indicated by blue arrows in Fig. 1(b)] along the yoz plane, respectively. Actually, the reflective metasurface can be used to independently manipulate the LCP or

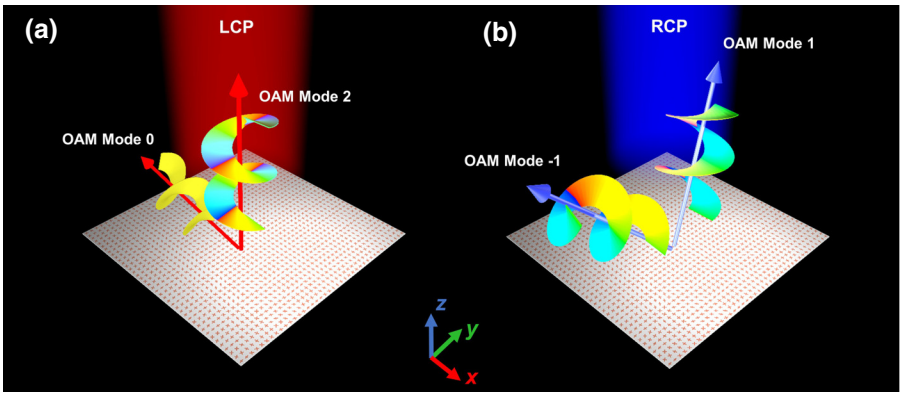

FIG. 1. The schematic of a bifunctional reflective metasurface dependent on the helicity. (a) For the LCP incidence, the reflective beams are generated to have OAM $l=2$ toward the normal direction and OAM mode $l=0$ (pencil beam) toward the $-x$ direction with deviation angle 51°. (b) For RCP incidence, two vortex beams carrying OAM $l=1$ (-1) will be deflected toward the direction of $-11°$ $(+23°)$ along the *yoz* plane. (indicated by arrows in the centere).

RCP wavefront in a way by the use of judiciously predesigned phase profiles, thus ultimately generating distinct and independent OAM states for incidence with different helicities.

While metasurfaces operating in the reflection mode could provide possibilities to realize extreme high efficiency and improved bandwidth within subwavelength thicknesses [8,13], most of the previous works are focused on independent control over the CP wavefronts in transmission mode. Here, we develop a general theory to analyze metasurface elements operated in the reflection mode and find the analytical solutions required for reflective dual-helicity decoupled wavefront control. We define the incident and reflected electric field vectors as $\mathbf{E^i}$ and $\mathbf{E^r}$, respectively. The vector $\mathbf{E^i}$ consists of two orthogonal CP wave-front components $\mathbf{E^i_L}$ and $\mathbf{E^i_R}$, which can be written as a form of $\mathbf{E^i} = (\mathbf{E^i_L}\mathbf{E^i_R})^{\mathrm{T}}$. Similarly, the vector $\mathbf{E^r}$ can be expressed as $\mathbf{E^r} = (\mathbf{E^r_L}\mathbf{E^r_R})^{\mathrm{T}}$. For a normal incidence case, the reflection matrix is defined as $\mathbf{R}$. Thus, the reflected electric field can be further calculated by the reflection matrix as $\mathbf{E^r} = \mathbf{RE^i}$,

$$\begin{pmatrix} \mathbf{E^r_L} \\ \mathbf{E^r_R} \end{pmatrix} = \begin{pmatrix} R_{LL} & R_{LR} \\ R_{RL} & R_{RR} \end{pmatrix} \begin{pmatrix} \mathbf{E^i_L} \\ \mathbf{E^i_R} \end{pmatrix}. \tag{1}$$

Here, R_{LL}, R_{LR}, R_{RL}, and R_{RR} represent the reflection coefficients, where the first subscript indicates the polarization state of the reflective wave and the second subscript indicates the incident polarization. The reflection matrix $\mathbf{R}$ for an arbitrary structure containing both propagation and geometric phases in a helicity basis can be written as

$$\mathbf{R} = \begin{pmatrix} R_{LL} & R_{LR} \\ R_{RL} & R_{RR} \end{pmatrix} = \begin{pmatrix} \eta e^{-i2\alpha} & \delta \\ \delta & \eta e^{i2\alpha} \end{pmatrix}, \tag{2}$$

where the local part of the reflection field δ and the converted part η can be calculated as $\delta = (R_x e^{i\varphi x} + R_y e^{i\varphi y})/2$ and $\eta = (R_x e^{i\varphi x} - R_y e^{i\varphi y})/2$. The R_x, R_y, φ_x, and φ_y indicate the reflection amplitude and reflection phase for a linearly x and y polarized em wave, respectively [10]. The α is the angular orientation of the meta-atom. From reflection matrix $\mathbf{R}$, it can be clearly observed that the reflection characteristics not only relate to the linear propagation response, but also the spatial variation α of the meta-atom. If the reflection amplitudes of the meta-atom are kept as unity $(R_x = R_y = 1)$ for both linearly polarized incidences but with a π phase difference $(\varphi_x - \varphi_y = \pi)$, the local part δ can be well suppressed to zero $(\delta = 0)$ while the converted part η can be reduced to $\eta = (e^{i\varphi x} - e^{i(\varphi x - \pi)})/2 = e^{i\varphi x}$. Therefore, the reflection matrix $\mathbf{R}$ can be simplified as

$$\mathbf{R} = \begin{pmatrix} e^{i(\varphi_x - 2\alpha)} & 0 \\ 0 & e^{i(\varphi_x + 2\alpha)} \end{pmatrix}. \tag{3}$$

Then the reflected electric field can be written as

$$\begin{pmatrix} \mathbf{E^r_L} \\ \mathbf{E^r_R} \end{pmatrix} = \begin{pmatrix} e^{i(\varphi_x - 2\alpha)}\mathbf{E^i_L} \\ e^{i(\varphi_x + 2\alpha)}\mathbf{E^i_R} \end{pmatrix}. \tag{4}$$

From the above equation we can clearly see that the reflected LCP and RCP waves are imparted with an additional phase of $\varphi_L = \varphi_x - 2\alpha$ and $\varphi_R = \varphi_x + 2\alpha$, respectively. Subtracting φ_L from φ_R, the spatial variation α can be obtained by

$$\alpha = (\varphi_R - \varphi_L)/4. \tag{5}$$

Due to the π phase difference between the x and y polarized reflected phase responses $(\varphi_x - \varphi_y = \pi)$, the reflection phase for linear x and y polarized incidences can be derived as

$$\varphi_x = (\varphi_L + \varphi_R)/2, \tag{6}$$

$$\varphi_y = (\varphi_L + \varphi_R)/2 - \pi. \tag{7}$$

Therefore, Eqs. (1) and (2) establish the relations between the propagation phase and geometric phase of a metastructure operating in reflection mode. For an arbitrary set of φ_L and φ_R, one just needs to design the φ_x, φ_y, and α according to the above equations. In other words, we can arbitrarily and independently manipulate the LCP and RCP reflection phases by designing three parameters: the

x polarized reflection phase φ_x, the y polarized reflection phase φ_y, and the rotation angle α. This would further allow a free combination of completely independent OAM functions for orthogonal incident CP wavefronts.

Since the phase tuning of a CP wave is closely dependent on reflection responses for linear polarization waves, cross talk for linearly polarized waves should be seriously suppressed, especially for metasurfaces with close spatial element distribution. This cross talk, if not well suppressed, will further lead to certain distortions of phase profiles for CP waves, as well as increase the complexity of the element optimization, because in this case, we should implement dual or even multiple parametric scanning to meet the phase requirement. On the contrary, if the metasurface element is designed with independent phase responses for two linearly polarized waves, we could directly design the structure parameters at once, releasing the burden caused by the polarization cross talk. Therefore, the complexity of the design process for CP wavefront incidence will be much reduced.

To verify the analytical solutions, we design a reflective coding metasurface element in the microwave region with a multilayer configuration, which can offer an independent control of the phase responses for two orthogonal linear polarizations. The meta-atom consists of three copper layers with a thickness of 0.018 mm, separated by two dielectric layers. The two dielectric spacers (Taconic TRF-43) have the same thickness of $h = 1.63$ mm, with a relative permittivity and loss tangent of 4.3 and 0.0035, respectively. The geometrical parameters of the meta-atom are shown in Fig. 2(a), in which $a = 1$ mm and $p = 6$ mm. The ground plane is used as the bottom layer to totally block the wave transmission to enable the reflection operation. Physical dimensions of the top metallic cruciform resonator are 90% of those of the second-layer metallic pattern. This tapered structure could offer more degrees of freedom in designing the necessary reflection phases and possibly extend the working bandwidth. With the rotation angle α fixed to be 0°, the reflected propagation phase responses for two linear polarizations are mainly determined by the parameters l_x and l_y, respectively. When the parameters l_y and α are fixed to be 2 mm and 0°, the reflection phase for the x polarized plane wave can be manipulated by varying the parameter l_x. It is clearly observed from Fig. 2(b) that as the l_x gradually increases from 1 to 5 mm, the reflected phase correspondingly decreases from about 360° to 0°, while the reflection amplitude always stays at high levels (more than 93%) within the frequency band from 14 to 18 GHz. At the same time, for y polarization, both reflection amplitude and phase are nearly immune from the

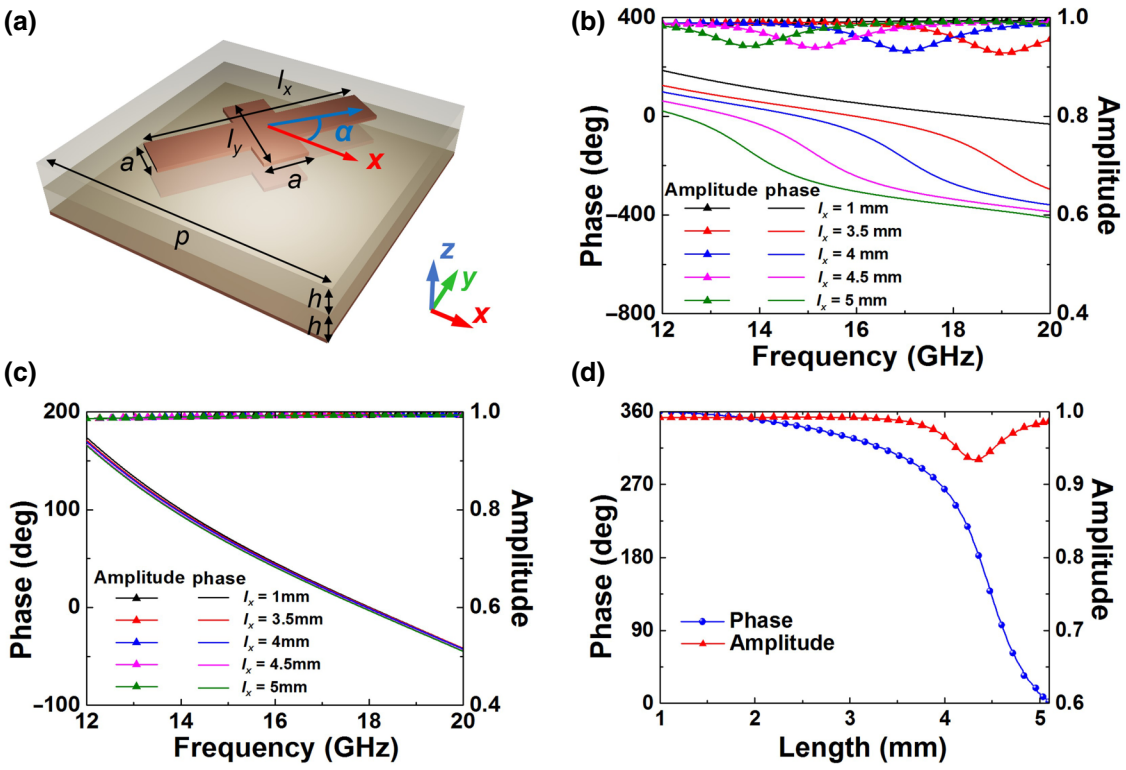

FIG. 2. (a) Schematic of the element combining the propagation phase and geometric phase. Simulated reflection amplitudes and phase responses of the element with different dimensions l_x for (b) x polarization, (c) y polarization from 12 to 20 GHz, with the rotation angle α fixed to be 0°. (d) Simulated reflection amplitude and phase responses of the element with different dimensions l_x (l_y) for x (y) polarization at 16 GHz.

change of parameter l_x, indicating that the meta-atom has very low cross talk between two orthogonal linear polarizations [shown in Fig. 2(c)]. Similar results can be obtained when the parameter l_x remains unchanged but l_y varies. Thus, the reflection phase for each linear polarization can be controlled independently by just changing l_x or l_y, while the reflection amplitude is always close to unity. Changing other physical parameters of the meta-atom can also have an influence on its phase functions, and even higher reflection efficiency may be obtained by simultaneously optimizing several parameters. However, only changing one parameter (l_x or l_y) while keeping other parameters unchanged will greatly reduce the complexity of the optimization process due to the phase functions monotonously decreasing with the parameters l_x or l_y [shown in Fig. 2(d)]. As l_x (or l_y) changes from 1 to 5 mm, the reflection phase can gradually decrease and cover a full 360° at a center frequency of 16 GHz, and at the same time, the reflection amplitude uniformly keeps exceeding 0.93.

Then we transform this meta-atom into a digital and coding metasurface element working for a CP wavefront to simply the design process by discretizing the phase responses. Here, we consider a coding metasurface with a 3-bit configuration. Therefore, the phase coverage from 0° to 360° is discretized into eight states with intervals of 45° at the operational frequency of 16 GHz [38]. The digital coding bytes "0," "1," "2," "3," "4," "5," "6," and "7" (or termed as "000," "001," ..., "111") are used to characterize the reflection phases of 0°, 45°, 90°, 135°, 180°, 225°, 270°, and 315°, respectively. The physical dimensions and

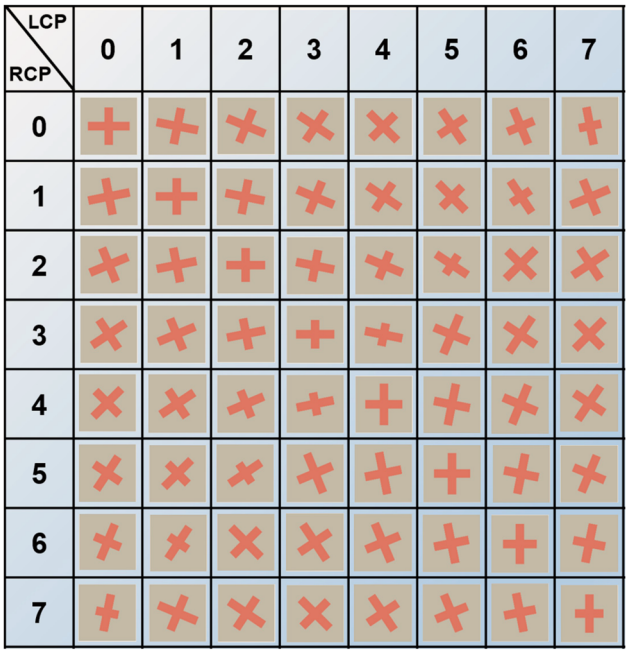

FIG. 3. The elements for 3-bit coding codes under LCP and RCP wave illumination.

the rotation angle of the meta-atom required for each coding element can be conveniently obtained by calculating Eqs. (5)–(7) and searching the design chart shown in Fig. 2(d). The aim here is to realize independent coding states for two CP wavefront incidences on a single meta-atom, so we have a total of 64 metasurface elements by combining the eight states for the LCP wave and eight states for the RCP wave, as shown in Fig. 3. Since the absolute phase shift for a certain meta-atom is dispersive, the definition of the coding element is normalized to the reflection phase of the digital state "0/0" for simplicity. For example, when the digital state for the LCP and RCP wave is "3/4," the spatial variation of the meta-atom is $\alpha = 11.25°$ and the parameters $l_x = 4.43$ mm ($l_y = 2.67$ mm) correspond to the linear phase response $\varphi_x = 157.5°$ ($\varphi_y = 337.5°$) at 16 GHz, respectively. These 3-bit coding elements, when combined together with predesigned spatial distributions, can permit helicity controlled dual-functional OAM performances and, in general, any of the achievable functions supported by these elements can freely be integrated onto a single metasurface design in a helicity switchable manner.

III. METASURFACE DESIGN AND SIMULATION RESULTS

To verify the feasibility of the theoretical model and interpret the design process, we show several coding metasurfaces designed for generating helicity selective OAM and their corresponding full-wave simulation results. For a 3-bit coding metasurface, five OAM mode states $l = 0$, ± 1, and ± 2 can be independently encoded into two helical channels. At the same time, we can flexibly multiplex and anomalously redirect the OAM beams by introducing certain spatial phase gradients across the metasurface. Here, as the first example, we show that spin-preserved twin vortex beams with OAM modes $l = 1$ and $l = 0$ can be trigged by LCP and RCP, respectively. Figure 4(a) or 4(b) shows the mixed coding pattern for generating twin vortex beams in the *xoz* or *yoz* planes under the illumination of LCP or RCP incidence, respectively, whose detailed configuration is shown in Fig. S1 of the Supplemental Material [51]. The metasurface is first divided into eight sectors and the circumferential phase interval between adjacent sectors is 45° (Fig. S1(a) in the Supplemental Material [51]). Thus, a vortex beam with OAM mode $l = 1$ can be generated by a metasurface with this coding pattern. In order to obtain two symmetric vortex beams in the *xoz* plane, a periodic coding pattern of "0 0 0 4 4 4⋯" along the *x* direction should be encoded onto the metasurface (Fig. S1(b) in the Supplemental Material [51]). Such an interleaved phase profile can lead to destructive interference along the surface normal direction in the far-field region, while constructive interference along the predesigned directions deviates from the *z* direction. The mixed coding pattern

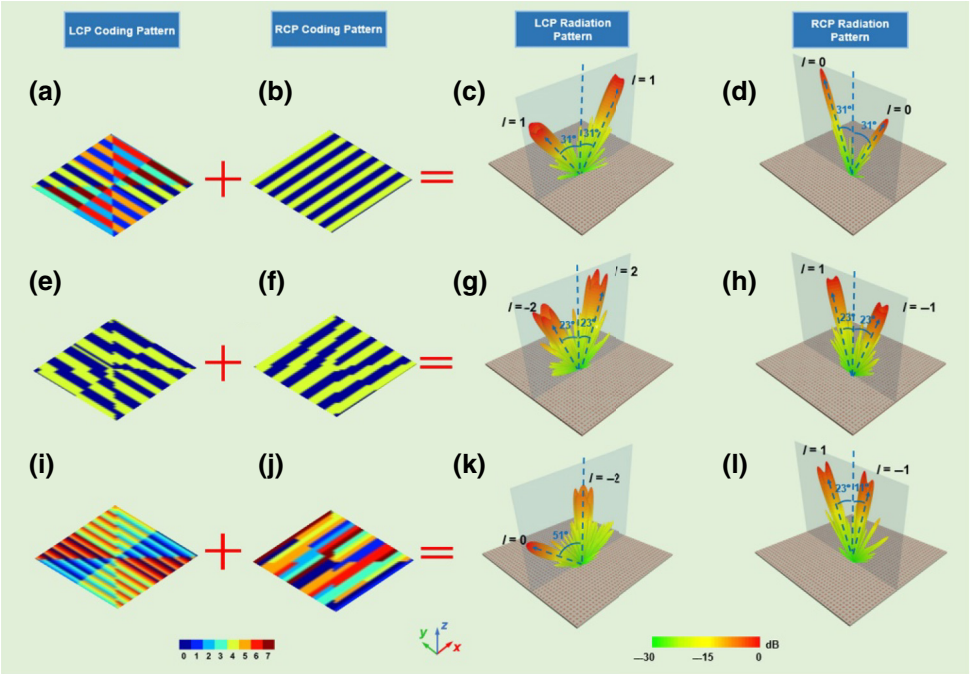

FIG. 4. Performances of the proposed coding metasurfaces for dual-helicity decoupled em wave control. Three coding metasurfaces are given: (a, e, i) Coding patterns for LCP incident wave. (b, f, j) Coding patterns for RCP incident wave. (c, g, k) Simulated 3D scattering patterns of the coding patterns in (a), (e), and (i) for the LCP incidence at 16 GHz. (d, h, l). Simulated 3D scattering patterns of the coding patterns in (b), (f), and (j) for the RCP incidence at 16 GHz.

is shown in Fig. S1(c) of the Supplemental Material [51], which can be viewed as the convolution operation [49]. As for RCP incidence, a similar periodic coding pattern "0 0 0 4 4 4⋯" along the y direction (Fig. S2(b) in the Supplemental Material [51]) is applied to obtain twin beams with an OAM mode $l=0$ in the yoz plane. The anomalous reflection angle of the beams can be calculated by the generalized Snell's reflection law [5]

$$\sin(\theta_r) - \sin(\theta_i) = \frac{\lambda_0}{2\pi}\frac{d\Phi}{dl}, \tag{8}$$

where the θ_i and θ_r represent the incident angle and anomalous reflection angle of the em wave, respectively, and λ_0 is the working wavelength in vacuum (corresponding frequency f_0). The phase gradient $d\Phi/dl$ can be calculated by the interleaved spatial phase and the lattice size. In this scheme, the deviation angle of the beams apart from the z axis is 31.4°, with the working frequency set as 16 GHz. Then we can conveniently design the spatial distribution of metasurface elements (shown in Fig. S2(c) of the Supplemental Material [51]) by searching the design table shown in Fig. 3. The corresponding normalized 3D far-field scattering patterns under LCP and RCP illuminations are shown in Figs. 4(c) and 4(d), respectively, where the anomalous reflection angles are in good agreement with the theoretical predictions. Meanwhile, the directivity property of the proposed metasurface, which is the key to further applications [50], has been discussed in section II of the Supplemental Material [51].

Actually, em wave-carrying multiple orthogonal OAM modes can greatly enhance the capacity of information communication and further increase its practicality. We can use the proposed coding metasurface to generate vortex beams with multiple orthogonal OAM modes, quite distinct for LCP and RCP incidences. Then we design the second example, which possesses twin beams carrying OAM modes with conjugate values. To obtain this kind of metasurface, we design a coding pattern (OAM mode $l=2$) containing eight discrete sectors, with phase intervals between adjacent sectors of 90° (Fig. S3(a) in the Supplemental Material [51]). We should do a convolution operation between the OAM coding pattern and a constant phase gradient coding pattern of "7 6 5 4 3 2 1 0" along the x direction, as shown in Fig. S3(c) of the Supplemental Material [51]. Then, a vortex beam ($l=2$) with an anomalous refraction angle of 23° at 16 GHz can be obtained by this coding pattern. Similarly, a coding pattern with the opposite OAM mode $l=-2$ (Fig. S3(d) in the Supplemental Material [51]) is added with a coding gradient "0 1 2 3 4 5 6 7" along the x direction (Fig. S3(e) in the Supplemental Material [51]). The vortex beam with an OAM mode $l=-2$ can be anomalously refracted to $-23°$ along the x direction at 16 GHz by this mixed coding pattern (Fig. S3(f) in the Supplemental Material [51]). In order to obtain a function-integrated metasurface for generating a dual-OAM wave, we should further do complex coding addition by [23]

$$e^{j\Phi_1(x,y)} + e^{j\Phi_2(x,y)} = A_0 e^{j\Phi_0(x,y)}, \tag{9}$$

where $\Phi_1(x, y)$ and $\Phi_2(x, y)$ represent the coding phase distributions of two independent functions on the metasurface, respectively. With the complex coding addition

operation as shown in Eq. (9), we can get a new complex coding phase distribution $\Phi_0(x, y)$ whose corresponding function is the superposition of the two aforementioned independent functions. Thus, the final coding pattern for LCP incidence is shown in Fig. 4(e), and the corresponding 3D far-field scattering pattern is shown in Fig. 4(g), where $l = \pm 2$ vortex beams with anomalous reflection angles of $\pm 23°$ deviated from the z axis in the xoz plane can be obtained. The design process of the coding pattern for the RCP wave is shown in Fig. S4 of the Supplemental Material [51]. A coding pattern with OAM mode $l = 1/-1$ is added with a coding gradient "7 6 5 4 3 2 1 0"/"0 1 2 3 4 5 6 7" along the y direction. Then, operating complex coding addition between these two coding patterns according to Eq. (9), we can obtain the final coding pattern for RCP incidence [Fig. 4(f)] and the corresponding layout of the coding metasurface (Fig. S5 in the Supplemental Material [51]). Such a metasurface with a mixed coding pattern for RCP incidence will result in a far-field scattering pattern of a two-beam-carrying OAM mode $l = \pm 1$, accompanied by anomalous refraction angles of $\pm 23°$ deviated from the z axis in the yoz plane, as illustrated in Fig. 4(h). Therefore, the vortex beams carrying OAM mode $l = \pm 2/\pm 1$ for LCP and RCP incidence can be generated by a single metasurface.

Without loss of generality, we also design a metasurface that can generate multiple vortex beams with simultaneously different OAM modes and distinct anomalous refraction angles in a helicity-selective manner [Figs. 4(i)–4(l)]. As shown in Fig. S6 of the Supplemental Material [51], a coding pattern with OAM mode $l = -2$ is complexly added with a gradient coding pattern "0 2 4 6 0 2 4 6" along the x direction for LCP incidence. Thus, the vortex beams carrying OAM modes $l = -2$ and $l = 0$ are emitted with deviation angles of 0° and 51°, respectively. For RCP incidence, a convolution operation of coding pattern (for OAM mode $l = 1$) is added with a gradient coding pattern "7 6 5 4 3 2 1 0" varying along the y direction as shown in Figs. S7(a)–S7(c) of the Supplemental Material [51]. Meanwhile, a mixed coding pattern (Fig. S7(f) in the Supplemental Material [51]) is obtained by adding a coding pattern with OAM mode $l = -1$ (Fig. S7(d) in the Supplemental Material [51]) with a gradient coding pattern "0 0 1 1 2 2 3 3 4 4 5 5 6 6 7 7" along the y

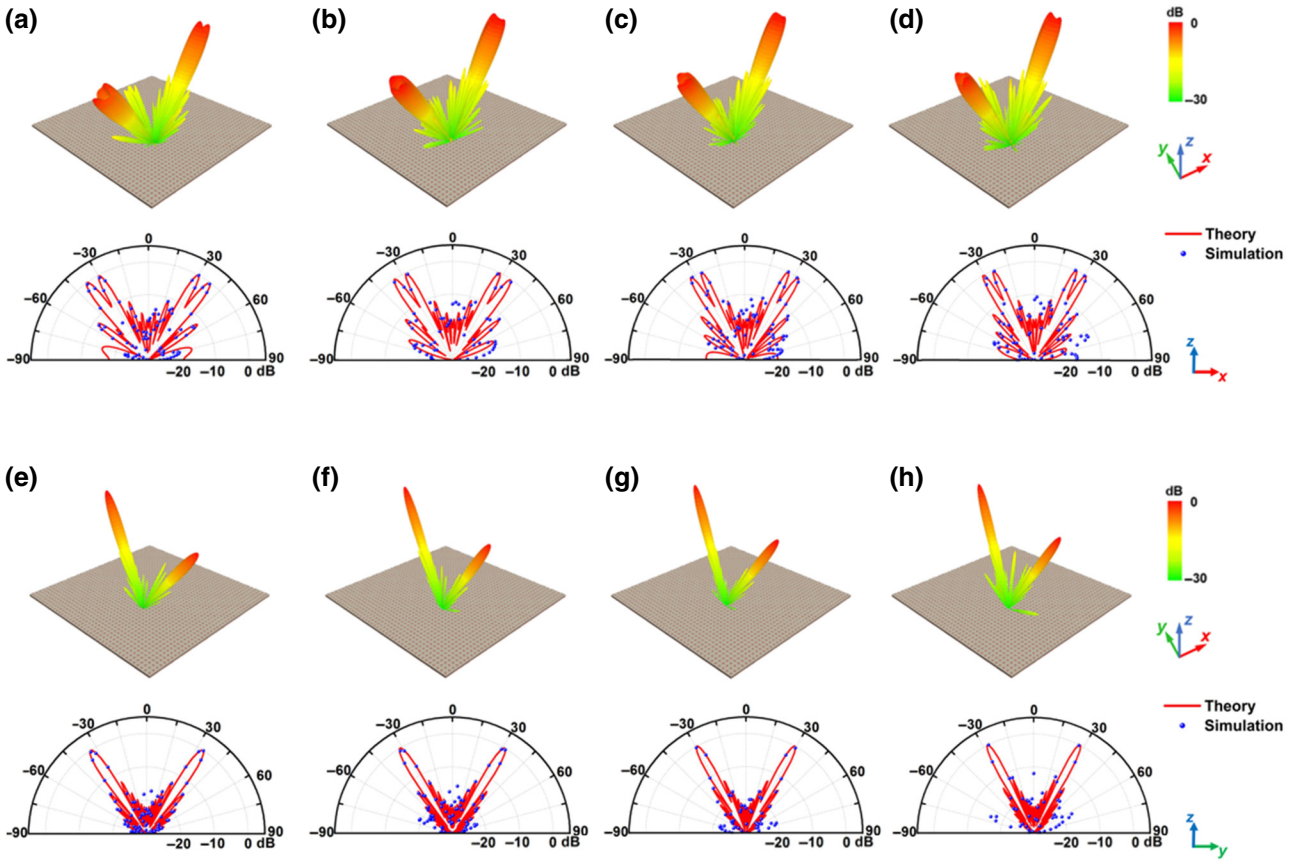

FIG. 5. The normalized 3D scattering patterns under LCP incident wave at (a) 15 GHz, (b) 16 GHz, (c) 17 GHz, and (d) 18 GHz. The bottom panels show the corresponding theoretical and simulated normalized 2D scattering patterns of the xoz plane. The normalized scattering patterns under RCP incident wave at (e) 15 GHz, (f) 16 GHz, (g) 17 GHz, and (h) 18 GHz. The bottom panels show the corresponding theoretical and simulated normalized 2D scattering patterns of the yoz plane.

direction (Fig. S7(e) in the Supplemental Material [51]). The RCP coding pattern is the complex addition operation of the two former coding patterns (Figs. S7(c) and S7(f) in the Supplemental Material [51]). Combining it with the mixed coding pattern shown in Fig. S6(c) of the Supplemental Material for the LCP wave [51], a pencil beam and a vortex beam with OAM mode $l=-2$ (two vortex beams with OAM mode $l=1$ and -1) are scattered with the deflection angles of 51° and 0° (23° and −11°) along the x (y) direction for the LCP (RCP) wave by the designed multifunctional metasurface, as shown in Figs. 4(k) and 4(l). These simulated results shown in Figs. 4(c), 4(d), 4(g), 4(h), 4(k), and 4(l) demonstrate that the proposed reflective coding metasurface offers an alternative method to independently design multiple OAM modes under orthogonal helicity. Although only five OAM modes are proposed here, the proposed metasurface can generate more OAM modes and more complex functionalities by involving more discrete meta-atoms.

For the metasurface shown in Fig. S2 of the Supplemental Material [51], the bandwidth performance is analyzed by simulating the 3D normalized far-field scattering

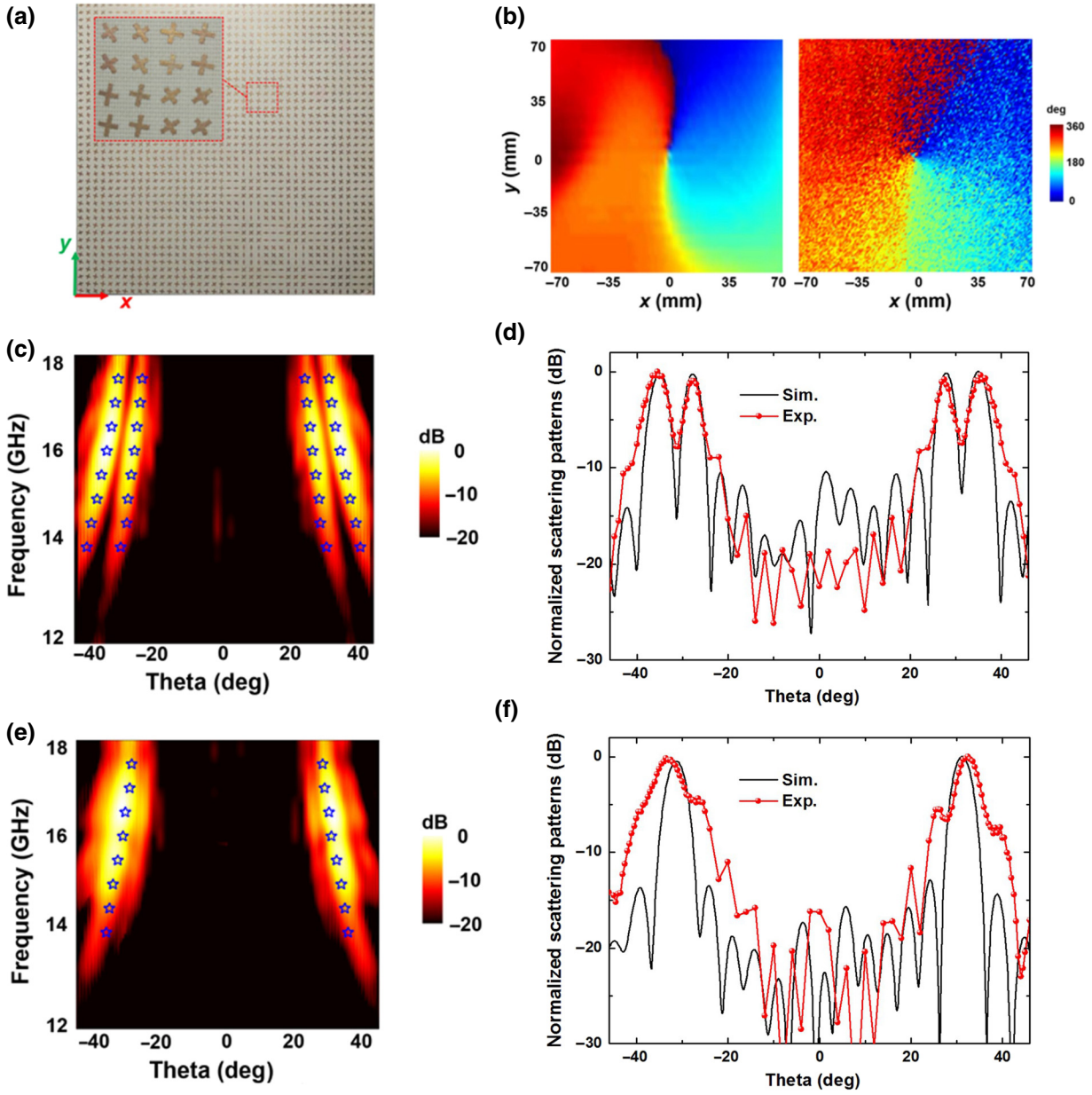

FIG. 6. (a) Fabricated sample of coding metasurface. (b) Simulated and measured near-field distributions of the metasurface at 16 GHz. (c, d) Measured and simulated results of 2D normalized scattering patterns from 12 to 18 GHz and corresponding 2D results at 16 GHz in the *xoz* plane. (e, f) Measured and simulated results of 2D normalized scattering patterns from 12 to 18 GHz and corresponding 2D results at 16 GHz in the *yoz* plane.

patterns under the normal illumination of a LCP or RCP wave at different frequencies as shown in Figs. 5(a)–5(h), and the bottom panels show the corresponding theoretical and simulated normalized two-dimensional (2D) scattering patterns. As the working frequency increases from 15 to 18 GHz with an interval of 1 GHz, the simulated deflection angles of the vortex beams and pencil beams are 33.5°, 31°, 29°, and 27°, respectively, which is consistent with the theoretical calculations. It obviously shows that the em waves emitted from the encoded metasurface are two symmetric vortex beams for the LCP wave and two pencil beams in the orthogonal direction for the RCP wave in a broad operation frequency bandwidth. As for higher OAM modes, the metasurface can still generate twin beams carrying OAM modes, but the sidelobe levels will slightly increase, resulting in a slightly reduced working band.

IV. EXPERIMENTAL VERIFICATION

To experimentally validate the proposed method and designed metasurface, one sample of the reflective coding metasurface is fabricated. The coding metasurface can be fabricated employing the printed circuit board (PCB) technique. The photograph of the fabricated metasurface corresponding to the designed one [Figs. 4(c) and 4(d)] is shown in Fig. 6(a), which includes 40×40 coding elements resulting in a total area of 240×240 mm^2 and an enlarged view of the metasurface elements is shown in the inset. The corresponding coding metasurface generates two symmetrical vortex beams with OAM mode $l = 1$ in the *xoz* plane under LCP incident illumination and two pencil beams ($l = 0$) in the *yoz* plane under RCP incident illumination and the deviation angles θ of all four beams are designed as 31° at 16 GHz. The 3D em field-scanning system is used to measure the phase distribution of the reflected electric field at the operational frequency of 16 GHz. The measured plane is set at a section perpendicular to the direction with a deviation angle $\theta = 31°$ in the *xoz* plane and it is set at a distance of $d = 1$ m (approximately $53\lambda_0$) away from the center of the metasurface. The observation area is about 140×140 mm^2. The measured phase distribution in Fig. 6(b) clearly shows that the OAM mode number of the vortex beam is $l = 1$, which is consistent with the simulated phase distribution. We measure the scattering patterns of the sample in a standard microwave chamber and the measured results are calibrated to a same size metal plate. The simulated and measured scattering patterns in the *xoz* and *yoz* planes from 12 to 18 GHz are shown in Figs. 6(c) and 6(e), where the blue asterisks represent the peak angles at different frequencies obtained by simulations. The simulated and measured 2D *xoz* and *yoz* scattering patterns clearly show that two symmetric vortex beams and two symmetric pencil beams are generated along the *xoz* and *yoz* planes from 14 to 18 GHz, respectively. As the working frequency increases from 14 to 18 GHz, the elevation angles of the reflective beams change from 36° to 28°. In order to compare the simulated and measured results more clearly, we present the normalized scattering pattern of both orthogonal planes at 16 GHz in Figs. 6(d) and 6(f). All simulated radiation beams have deviation angles of 31° and the measured results are good matches with the simulated ones, which proves the feasibility of the proposed method.

V. CONCLUSION

In conclusion, we propose a dual-helicity decoupled coding metasurface that can independently encode distinct OAM vortices for two orthogonal helicities, realizing desired spin-to-OAM conversions. Guided by the proposed theoretical method, several design examples demonstrate that such coding metasurfaces could carry the desired independent OAM modes in a helicity-selective manner, which may significantly improve the information capacity of the metasurfaces. The simulated results have been verified by the microwave experiments, and good agreements are observed between them. The proposed method could offer an alternative path for independently tailoring CP wavefronts in a helicity-selective manner with high efficiency, which may find potential uses in many real-world applications, for example, wireless communication. The design principle can also be readily extended to other frequency bands, such as millimeter waves, terahertz waves, and even the optical regimes.

ACKNOWLEDGMENTS

This work is partially supported by the Priority Academic Program Development of Jiangsu Higher Education Institutions (PAPD), the Fundamental Research Funds for the Central Universities, and Jiangsu Provincial Key Laboratory of Advanced Manipulating Technique of Electromagnetic Wave. National Key Research and Development Program of China (Grant No. 2017YFA0700201); National Natural Science Foundation of China (NSFC) (Grants No. 61671231, No. 61801207, No. 61731010, and No. 61571218); China Postdoctoral Science Foundation (Grant No. 2017M620202).

[1] V. G. Veselago, The electrodynamics of substances with simultaneously negative values of ε and μ, Sov. Phys. Usp. **10**, 509 (1968).

[2] J. B. Pendry, A. J. Holden, D. J. Robbins, and W. J. Stewart, Magnetism from conductors and enhanced nonlinear phenomena, IEEE Trans. Microw. Theory **47**, 2075 (1999).

[3] J. B. Pendry, A. J. Holden, W. J. Stewart, and I. Youngs, Extremely Low Frequency Plasmons in Metallic Mesostructures, Phys. Rev. Lett. **76**, 4773 (1996).

[4] R. A. Shelby, D. R. Smith, and S. Schultz, Experimental verification of a negative index of refraction, Science **292**, 77 (2001).

[5] N. Yu, P. Genevet, M. A. Kats, F. Aieta, J. P. Tetienne, F. Capasso, and Z. Gaburro, Light propagation with phase discontinuities: generalized laws of reflection and refraction, Science **334**, 333 (2011).

[6] L. Liu, X. Zhang, M. Kenney, X. Su, N. Xu, C. Ouyang, Y. Shi, J. Han, W. Zhang, and S. Zhang, Broadband metasurfaces with simultaneous control of phase and amplitude, Adv. Mater. **26**, 5031 (2014).

[7] A. V. Kildishev, A. Boltasseva, and V. M. Shalaev, Planar photonics with metasurfaces, Science **339**, 1232009 (2013).

[8] S. Sun, Q. He, S. Xiao, Q. Xu, X. Li, and L. Zhou, Gradient-index meta-surfaces as a bridge linking propagating waves and surface waves, Nat. Mater. **11**, 426 (2012).

[9] L. Zhang, S. Liu, L. L. Li, and T. J. Cui, Spin-controlled multiple pencil beams and vortex beams with different polarizations generated by pancharatnam-berry coding metasurfaces, ACS Appl. Mater. Interfaces **9**, 36447 (2017).

[10] B. Wang, F. Dong, H. Feng, D. Yang, Z. Song, L. Xu, W. Chu, Q. Gong, and Y. Li, Rochon-prism-like planar circularly polarized beam splitters based on dielectric metasurfaces, ACS Photonics **5**, 1660 (2017).

[11] F. Zhang, M. Pu, X. Li, P. Gao, X. Ma, J. Luo, H. Yu, and X. Luo, All-dielectric metasurfaces for simultaneous giant circular asymmetric transmission and wavefront shaping based on asymmetric photonic spin-orbit interactions, Adv. Funct. Mater. **27**, 1704295 (2017).

[12] Z. Li, E. Palacios, S. Butun, and K. Aydin, Visible-frequency metasurfaces for broadband anomalous reflection and high-efficiency spectrum splitting, Nano Lett. **15**, 1615 (2015).

[13] S. Sun, K. Y. Yang, C. M. Wang, T. K. Juan, W. T. Chen, C. Y. Liao, Q. He, S. Xiao, W. T. Kung, and G. Y. Guo, High-efficiency broadband anomalous reflection by gradient meta-surfaces, Nano Lett. **12**, 6223 (2012).

[14] H. Cheng, S. Chen, P. Yu, W. Liu, Z. Li, J. Li, B. Xie, and J. Tian, Dynamically tunable broadband infrared anomalous refraction based on graphene metasurfaces, Adv. Opt. Mater. **3**, 1744 (2016).

[15] F. Ding, Z. Wang, S. He, V. M. Shalaev, and A. V. Kildishev, Broadband high-efficiency half-wave plate: a supercell-based plasmonic metasurface approach, ACS Nano **9**, 4111 (2015).

[16] D. Wang, Y. Gu, Y. Gong, C. W. Qiu, and M. Hong, An ultrathin terahertz quarter-wave plate using planar babinet-inverted metasurface, Opt. Express **23**, 11114 (2015).

[17] K. Chen, Y. Feng, F. Monticone, J. Zhao, B. Zhu, T. Jiang, L. Zhang, Y. Kim, X. Ding, and S. Zhang, A reconfigurable active huygens' metalens, Adv. Mater. **29**, 1606422 (2017).

[18] S. M. Kamali, E. Arbabi, A. Arbabi, Y. Horie, and A. Faraon, Highly tunable elastic dielectric metasurface lenses, Laser Photonics Rev. **10**, 1002 (2016).

[19] G. Zheng, H. Muhlenbernd, M. Kenney, G. Li, T. Zentgraf, and S. Zhang, Metasurface holograms reaching 80% efficiency, Nat. Nanotechnol. **10**, 308 (2015).

[20] W. T. Chen, K. Y. Yang, C. M. Wang, Y. W. Huang, G. Sun, I. D. Chiang, C. Y. Liao, W. L. Hsu, H. T. Lin, and S. Sun, High-efficiency broadband meta-hologram with polarization-controlled dual images, Nano Lett. **14**, 225 (2014).

[21] X. Zhao, S. P. Yeo, and L. C. Ong, Decoupling of inverted-F antennas with high-order modes of ground plane for 5G mobile MIMO platform, IEEE Trans. Antennas Propag. **66**, 4485 (2018).

[22] I. Dioum, A. Diallo, S. M. Farsi, and C. Luxey, A novel compact dual-band LTE antenna-system for MIMO operation, IEEE Trans. Antennas Propag. **62**, 2291 (2014).

[23] R. Y. Wu, C. B. Shi, S. Liu, W. Wu, and T. J. Cui, Addition theorem for digital coding metamaterials, Adv. Opt. Mater. **6**, 1701236 (2018).

[24] L. H. Gao, Q. Cheng, J. Yang, S. J. Ma, J. Zhao, S. Liu, H. B. Chen, Q. He, W. X. Jiang, H. F. Ma, Q. Y. Wen, L. J. Liang, B. B. Jin, W. W. Liu, L. Zhou, J. Q. Yao, P. H. Wu, and T. J. Cui, Broadband diffusion of terahertz waves by multi-bit coding metasurfaces, Light-Sci. Appl. **4**, e324 (2015).

[25] L. Li, T. J. Cui, J. Wei, S. Liu, J. Ding, W. Xiang, Y. B. Li, M. H. Jiang, C. W. Qiu, and S. Zhang, Electromagnetic reprogrammable coding-metasurface holograms, Nat. Commun. **8**, 197 (2017).

[26] R. C. Devlin, A. Ambrosio, N. A. Rubin, J. B. Mueller, and F. Capasso, Arbitrary spin-to-orbital angular momentum conversion of light, Science **358**, 896 (2017).

[27] F. Bouchard, I. De Leon, S. A. Schulz, J. Upham, E. Karimi, and R. W. Boyd, Optical spin-to-orbital angular momentum conversion in ultra-thin metasurfaces with arbitrary topological charges, Appl. Phys. Lett. **105**, 101905 (2014).

[28] R. C. Devlin, A. Ambrosio, D. Wintz, S. L. Oscurato, A. Y. Zhu, M. Khorasaninejad, J. Oh, P. Maddalena, and F. Capasso, Spin-to-orbital angular momentum conversion in dielectric metasurfaces, Opt. Express **25**, 377 (2017).

[29] G. Ding, K. Chen, T. Jiang, B. Sima, J. Zhao, and Y. Feng, Full control of conical beam carrying orbital angular momentum by reflective metasurface, Opt. Express **26**, 20990 (2018).

[30] Y. Guo, M. Pu, Z. Zhao, Y. Wang, J. Jin, P. Gao, X. Li, X. Ma, and X. Luo, Merging geometric phase and plasmon retardation phase in continuously shaped metasurfaces for arbitrary orbital angular momentum generation, ACS Photonics **3**, 2022 (2016).

[31] D. Hakobyan, H. Magallanes, G. Seniutinas, S. Juodkazis, and E. Brasselet, Tailoring orbital angular momentum of light in the visible domain with metallic metasurfaces, Adv. Opt. Mater. **4**, 306 (2016).

[32] S. Yu, L. Li, G. Shi, C. Zhu, and Y. Shi, Generating multiple orbital angular momentum vortex beams using a metasurface in radio frequency domain, Appl. Phys. Lett. **108**, 241901 (2016).

[33] Z. H. Jiang, L. Kang, W. Hong, and D. H. Werner, Highly Efficient Broadband Multiplexed Millimeter-Wave Vortices from Metasurface-Enabled Transmit-Arrays of Subwavelength Thickness, Phys. Rev. Appl. **9**, 064009 (2018).

[34] Q. Ma, C. B. Shi, G. D. Bai, T. Y. Chen, A. Noor, and T. J. Cui, Beam-editing coding metasurfaces based on polarization bit and orbital-angular-momentum-mode bit, Adv. Opt. Mater. **5**, 1700548 (2017).

[35] L. Zhang, R. Y. Wu, G. D. Bai, H. T. Wu, Q. Ma, X. Q. Chen, and T. J. Cui, Transmission-reflection-integrated multifunctional coding metasurface for full-space controls of electromagnetic waves, Adv. Funct. Mater. **28**, 1802205 (2018).

[36] P. Chen, S. J. Ge, W. Duan, B. Y. Wei, G. X. Cui, W. Hu, and Y. C. Lu, Digitalized geometric phases for parallel optical spin and orbital angular momentum encoding, ACS Photonics **4**, 1333 (2017).

[37] Y. C. Zhang, W. W. Liu, J. Gao, and X. D. Yang, Generating focused 3D perfect vortex beams by plasmonic metasurfaces, Adv. Opt. Mater. **6**, 1701228 (2018).

[38] T. Stav, A. Faerman, E. Maguid, D. Oren, V. Kleiner, E. Hasman, and M. Segev, Quantum entanglement of the spin and orbital angular momentum of photons using metamaterials, Science **361**, 1101 (2018).

[39] D. Wen, F. Yue, W. Liu, S. Chen, and X. Chen, Geometric metasurfaces for ultrathin optical devices, Adv. Opt. Mater. **6**, 1800348 (2018).

[40] H. Gao, Y. Li, L. Chen, J. Jin, M. Pu, X. Li, P. Gao, C. Wang, X. Luo, and M. Hong, Quasi-Talbot effect of orbital angular momentum beams for generation of optical vortex arrays by multiplexing metasurface design, Nanoscale **10**, 666 (2018).

[41] Y. Li, X. Li, L. Chen, M. Pu, J. Jin, M. Hong, and X. Luo, Orbital angular momentum multiplexing and demultiplexing by a single metasurface, Adv. Opt. Mater. **5**, 1600502 (2017).

[42] F. Yue, D. Wen, C. Zhang, B. D. Gerardot, W. Wang, S. Zhang, and X. Chen, Multichannel polarization-controllable superpositions of orbital angular momentum states, Adv. Mater. **29**, 1603838 (2017).

[43] E. Maguid, I. Yulevich, D. Veksler, V. Kleiner, M. L. Brongersma, and E. Hasman, Photonic spin-controlled multifunctional shared-aperture antenna array, Science **352**, 1202 (2016).

[44] K. Chen, Y. Feng, Z. Yang, L. Cui, J. Zhao, B. Zhu, and T. Jiang, Geometric phase coded metasurface: from polarization dependent directive electromagnetic wave scattering to diffusion-like scattering, Sci. Rep. **6**, 35968 (2016).

[45] J. B. Mueller, N. A. Rubin, R. C. Devlin, B. Groever, and F. Capasso, Metasurface Polarization Optics: Independent Phase Control of Arbitrary Orthogonal States of Polarization, Phys. Rev. Lett. **118**, 113901 (2017).

[46] T. J. Cui, M. Q. Qi, X. Wan, J. Zhao, and Q. Cheng, Coding metamaterials, digital metamaterials and programmable metamaterials, Light Sci. Appl. **3**, e218 (2014).

[47] K. Chen, L. Cui, Y. Feng, J. Zhao, T. Jiang, and B. Zhu, Coding metasurface for broadband microwave scattering reduction with optical transparency, Opt. Express **25**, 5571 (2017).

[48] T. J. Cui, S. Liu, and L. L. Li, Information entropy of coding metasurface, Light Sci. Appl. **5**, e16172 (2016).

[49] S. Liu, T. J. Cui, L. Zhang, Q. Xu, Q. Wang, X. Wan, J. Q. Gu, W. X. Tang, M. Qing Qi, J. G. Han, W. L. Zhang, X. Y. Zhou, and Q. Cheng, Convolution operations on coding metasurface to reach flexible and continuous controls of terahertz beams, Adv. Sci. **3**, 1600156 (2016).

[50] S. Liu and T. J. Cui, Concepts, working principles, and applications of coding and programmable metamaterials, Adv. Opt. Mater. **5**, 1700624 (2017).

[51] See Supplemental Material at http://link.aps.org/supplemental/10.1103/PhysRevApplied.11.044043 for additional information on the design process of coding patterns cited in the main text, and directivity property of the proposed metasurface.